

Polymer Carpets

Ihsan Amin, Marin Steenackers, Ning Zhang, André Beyer, Xianghui Zhang, Tobias Pirzer, Thorsten Hugel, Rainer Jordan,* and Armin Götzhäuser*

The fabrication of defined polymer objects of reduced dimensions such as polymer-coated nanoparticles (zero-dimensional (0D)), cylindrical brushes (1D), and polymer membranes (2D), is currently the subject of intense research. In particular, ultrathin polymer membranes with high aspect ratios are being discussed as novel materials for miniaturized sensors because they would provide extraordinary sensitivity and dynamic range when sufficient mechanical stability can be combined with flexibility and chemical functionality. Unlike current approaches that rely on crosslinking of polymer layers for stabilization, this report presents the preparation of a new class of polymer material, so-called “polymer carpets,” a freestanding polymer brush grown by surface-initiated polymerization on a crosslinked 1-nm-thick monolayer. The solid-supported, as well as freestanding, polymer carpets are found to be mechanically robust and to react instantaneously and reversibly to external stimuli by buckling. The carpet mechanics and the dramatic changes of the film properties (optical, wetting) upon chemical stimuli are investigated in detail as they allow the development of completely new integrated micro-/nanotechnology devices.

Keywords:

- free-standing membranes
- nanosheets
- polymer brushes
- polymer carpets
- self-assembled monolayers

1. Introduction

Ultrathin, freestanding polymer membranes with macroscopic sizes and molecular thicknesses have received continuous interest in the past decade due to their potential as microsensors, actuators, or separation membranes.^[1–3] Various strategies have been developed for the design of defect-free and mechanically robust nanomembranes: layer-by-layer (LbL) assembly of polyelectrolyte multilayers,^[4,5] crosslinking of Langmuir–Blodgett^[6] and self-assembled monolayers (SAMs),^[7,8] self assembly of ABA triblock copolymers,^[9] and cast films.^[10] More recently, efforts have focused on enhancing the mechanical stability and elasticity of these polymeric nanomembranes. Tsukruk et al.^[11,12] showed that very robust 25–70-nm-thick membranes were accessible by embedding rigid nanoparticles within polymeric nanomembranes prepared by LbL assembly. Kunitake et al.^[13,14] developed different approaches for the preparation of 20–40-nm-thick mechanically stable nanomembranes by “high-density crosslinking” of a spincoated precursor solution. Due to their extraordinary sensitivity and dynamic range, highly crosslinked nanomembranes are regarded for next-generation pressure, thermal, tactile, and acoustic sensors.^[15,16] Polymer nanomembranes have recently entered the

[*] Dr. I. Amin, Dr. A. Beyer, Dr. X. Zhang, Prof. A. Götzhäuser

Physik Supramolekularer Systeme
Universität Bielefeld
Universitätsstraße 25, 33615 Bielefeld (Germany)
E-mail: goelzhaeuser@uni-bielefeld.de

Prof. R. Jordan
Professur für Makromolekulare Chemie
Technische Universität Dresden
Zellescher Weg 19, 01069 Dresden (Germany)
E-mail: Rainer.Jordan@tu-dresden.de

Dr. M. Steenackers, N. Zhang, Prof. R. Jordan
Wacker-Lehrstuhl für Makromolekulare Chemie
Technische Universität München
Lichtenbergstrasse 4, 85747 Garching (Germany)

Dr. M. Steenackers
Institute for Advanced Study
Technische Universität München
Arcisstrasse 21, 80333 München (Germany)

T. Pirzer, Prof. T. Hugel
Physikdepartment, IMETUM
Technische Universität München
Boltzmannstrasse 11, 85748 Garching (Germany)

DOI: 10.1002/sml.201000448

biomedical field as artificial nacre^[17] and as a novel material used in surgery.^[18] So far, a common feature of all developed freestanding polymer nanomembranes is the crosslinking of the polymer itself to ensure the mechanical stability of the layer. However, for the fabrication of chemical- or bioresponsive polymer-based nanomembranes, the high crosslinking naturally reduces the interactions between the polymer chains and the environment and thus impairs the sensitivity and flexibility of the films. Analogously to crosslinked polymer films versus polymer brushes on substrates, a brush reacts more quickly and has a higher sensitivity towards external stimuli. The entire layer has a better accessibility, even for larger molecules, and the strong chain stretching results in a considerably lower chain entanglement of the preorganized polymers along the surface normal. Hence, on surfaces, soft and stimuli-responsive polymer brushes have been the system of choice for the development of adaptive layers as actuators and sensors.^[19–23]

In this Full Paper, we report on the first freestanding polymer brush, grafted from a crosslinked monolayer (nanosheet) that provides mechanical stability and structural integrity. Because of the morphological similarity, we refer to this as a “polymer carpet.”

2. Results and Discussion

For the fabrication of polymer carpets, a ≈ 1 -nm-thin nanosheet was prepared by electron-beam-induced crosslinking of a biphenyl SAM. It was shown recently that these macroscopically large but ultrathin nanosheets are extremely stable both mechanically and thermally.^[8] After detachment of the crosslinked monolayer from the substrate and deposition onto a solid silicon support,^[8] the nanosheet was used as a two-dimensional (2D) template to grow a polymer brush by surface-initiated polymerization (SIP), forming the polymer carpet. Like a real carpet, a polymer carpet thus consists of a soft and flexible brush that is (covalently) attached to a thin and rigid 2D framework. The preparation of polymer brushes by SIP has been widely used during the past few decades and various strategies have been developed.^[20,21] Recently, we found that a specific surface-bound initiator is not needed and defined polymer brushes can be prepared by the self-initiated surface photopolymerization and photografting (SIPGP) of vinyl monomers.^[24–26] The preparation of polymer carpets is outlined in Figure 1.

In a first set of experiments, polymer carpets were prepared by SIPGP of styrene on approximately $5 \times 5 \text{ mm}^2$ crosslinked 4'-amino-1,1'-biphenyl-4-thiol (cABT) nanosheets supported on silicon wafers. The supported cABT was submerged in bulk styrene and irradiated with UV light at $\lambda_{\text{max}} = 350 \text{ nm}$, intensively rinsed with solvents of different polarities, dried in a jet of nitrogen, and investigated by atomic force microscopy (AFM) under ambient conditions.

As shown in Figure 2 and the insets of Figure 3, polystyrene (PS) was selectively grafted from the cABT nanosheets and no polymer was observed on the bare silicon wafer. The reactivity difference between the bare silicon substrate and the cABT nanosheet is in agreement with our previous

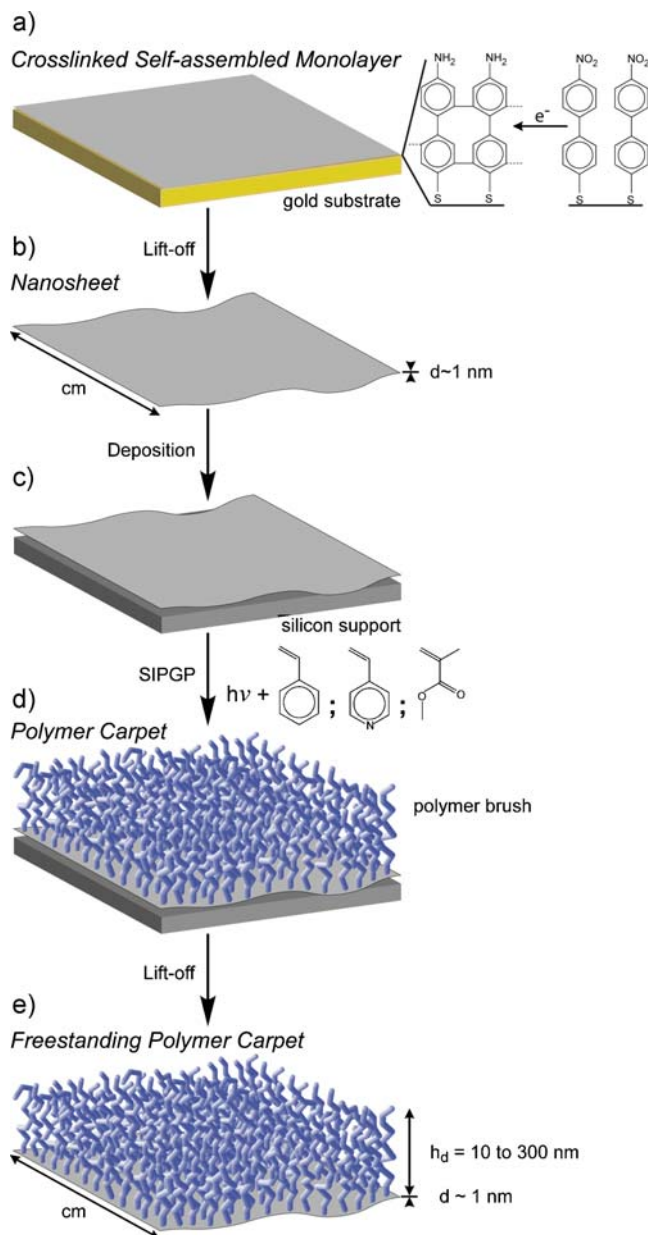


Figure 1. Scheme of the preparation of polymer carpets. a) A crosslinked cABT SAM is prepared by electron irradiation of NBT and b) detached by dissolving the gold substrate with a KI/I_2 solution. c) The nanosheet is deposited on a silicon substrate with thin silicon oxide or silicon nitride layer.^[8] d) Supported polymer carpets are obtained by SIPGP of a vinyl monomer (styrene, 4VP, or MMA). e) Freestanding polymer carpets are obtained by dissolving the underlying layer (Si_3N_4) with HF.

reports.^[24–26] The simpler approach of fabricating a polymer brush on the cABT SAMs, as we reported before, and then detaching the entire cABT/brush layer, which would also result in a polymer carpet, did not turn out to be successful in initial experiments.

The ex situ kinetic studies of the SIPGP for different UV-irradiation times (0.5–8 h) are summarized in Figure 3 (plot). The thickness development with the UV-irradiation time was found to be initially linear (35 nm h^{-1} between 0.5 and 4 h) with stagnation for longer irradiation times. This is in good

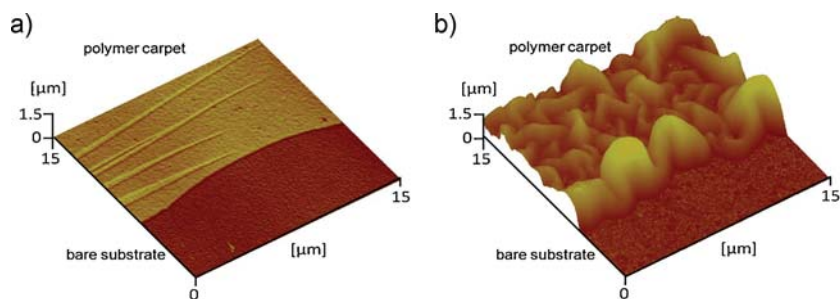


Figure 2. True-to-scale 3D representations of AFM measurements of PS-carpet edges on silicon: a) UV-irradiation time = 0.5 h, PS-nanocarpets thickness = 19 ± 7 nm; b) UV-irradiation time = 16 h. The PS nanocarpets thickness in (b) could not be determined accurately by AFM due to the high buckling amplitude (≈ 1.5 μm , rms).

agreement with our previous reports on SIPGP on SAMs^[24,25,27] and gives the direct possibility of modulating the polymer-brush thickness over a wide range.

Figure 4 shows 3D true-to-scale representations of the AFM scans of the supported PS carpets after different polymerization times. Detailed investigations of the PS-carpet morphology by AFM revealed that, for polymerization times below 1 h, homogeneous and very flat films were formed with a root-mean-square (rms) roughness of <2.5 nm (Figure 4a and b). For longer polymerization times and brush thicknesses (Figures 4c–f and 2b), the supported polymer carpets display significant buckling of increasing amplitude. This systematic morphology change is not due to, for example, inhomogeneous grafting but due to local detachment of the film from the solid support. Buckling of thin supported films is a known phenomenon^[28] and strain-induced buckling has been the subject of several studies.^[29–31] While, usually, buckling of thin films is induced by modulating an elastic support, here, a flexible polymer carpet is supported by a rigid substrate. The collapse of the polymer brush due to changes in the environment (from bulk monomer and good solvents used for carpet cleaning to air) results in significant stress within the film. Such stresses can occur due to

confinement effects in poor solvent conditions if the layer thickness is below the free extension of the chains.^[32,33] In such a case, the brush tends to develop instabilities, which can at least partially be compensated by crumpling of a flexible substrate. Since the flexible polymer brush is linked to a crosslinked nanosheet that cannot compensate for the lateral stress, the entire carpet locally detaches from the rigid support and buckles.

The PS carpets were further investigated by static (θ_s) and dynamic water-contact-angle measurements (Table 1). For thin and flat PS carpets, $\theta_s = 90$ – 95° as expected. However, with increasing film thickness and buckling, the surface roughness results in a high-contact-angle hysteresis (pinning) and advancing water-contact angle of 146° (superhydrophobicity).

Besides styrene, a broad variety of vinyl monomers can be grafted by the SIPGP process.^[25,34,35] This allows the preparation of polymer carpets with different properties and functionalities. So far, we have successfully prepared polymer carpets from methyl methacrylate (MMA) and 4-vinyl pyridine (4VP). Figure 5 displays the Fourier-transform infrared (FTIR) spectra of PS, P4VP, and PMMA carpets prepared as outlined in Figure 1. The FTIR spectrum of PS carpets display the characteristic stretching vibrational modes of the phenyl group (ν_{CH} at around 3023 cm^{-1} and ν_{CC} between 1446 , 1490 , and 1597 cm^{-1}) and the methylene groups of the polymer backbone with a maximum around 2929 cm^{-1} .

The spectrum of the P4VP carpets shows typical absorption bands, such as the aliphatic and aromatic $\nu_{\text{C-H}}$ stretching vibrations around 3021 cm^{-1} and the vibrational bands from the C=C double bonds of the pyridine ring at 1598 cm^{-1} . For PMMA carpets, the carbonyl stretching mode around 1724 cm^{-1} and aliphatic $\nu_{\text{C-H}}$ stretching vibrations at 2946 cm^{-1} can be assigned.

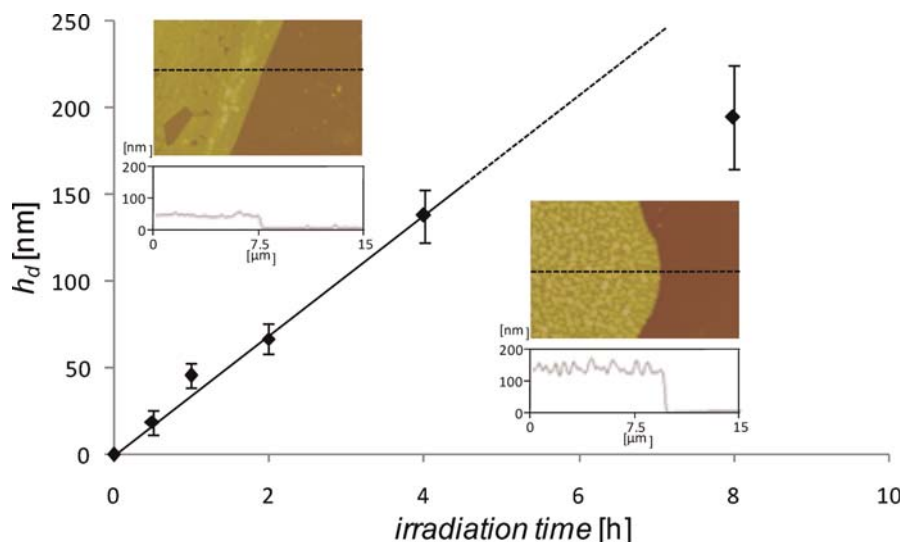


Figure 3. Ex situ kinetics of the thickness of dry PS carpets (h_d) as a function of the UV-irradiation time (0.5–8 h) on silicon-supported cABT nanosheets, as measured by AFM. The insets show AFM height images and section analysis of PS-carpet edges after polymerization times of 1 h (left) and 4 h (right). Because of carpet buckling, the layer thickness after 16 h could not be reliably determined by AFM.

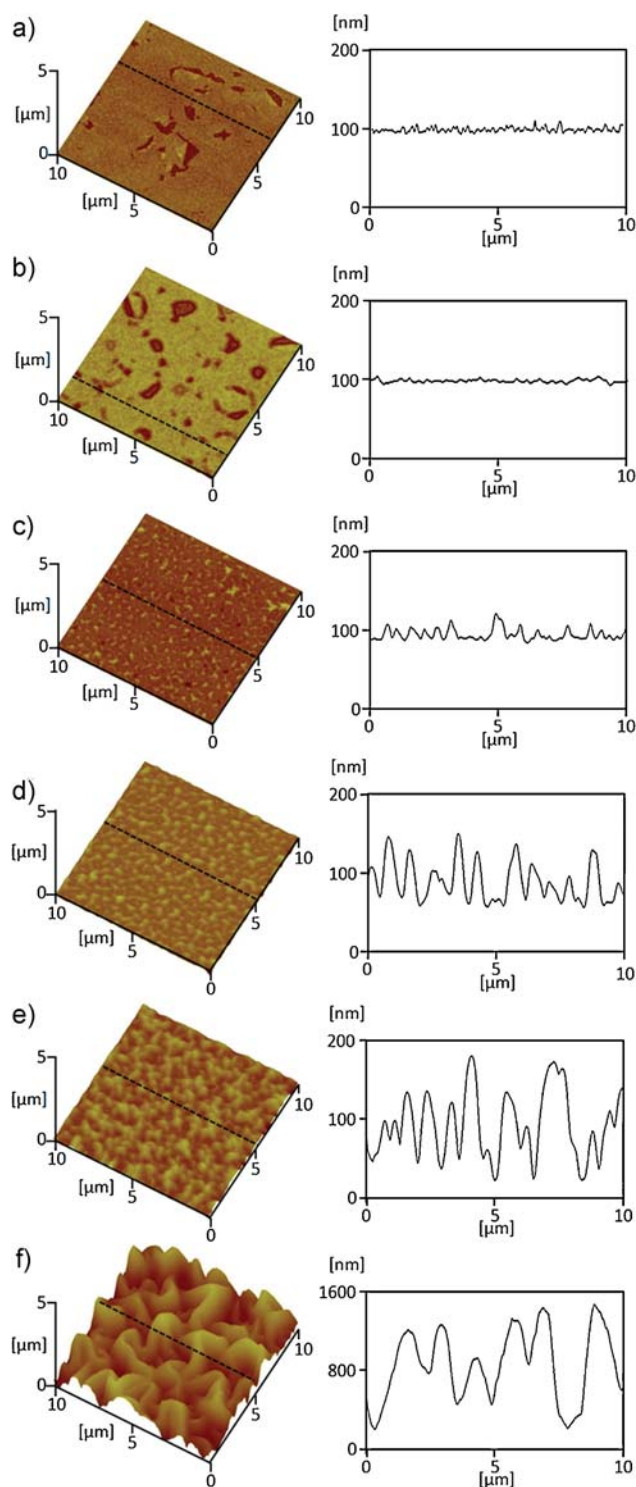


Figure 4. True-to-scale 3D representations and section analysis of AFM measurements of polymer carpets prepared by SIPGP of styrene on silicon-supported cABT nanosheets for a) 0.5, b) 1, c) 2, d) 4, e) 8, and f) 16 h.

The growth rate of the thickness of the polymer carpet was found to be specific for each monomer and to correlate roughly with the rate of free-radical polymerization of the respective monomer in solution. For example, after $t_p = 3$ h, MMA gave a 485 ± 18 -nm-thick PMMA carpet and 4VP gave a P4VP-carpet

thickness of 150 ± 11 nm after 19 h of irradiation, as determined by AFM.

The above-described significant buckling response of the PS carpet to good and bad solvents can be used to sense the solvent quality directly, as well as the pH with P4VP carpets. Silicon-supported P4VP carpets were investigated by AFM in ethanol as a good solvent. As expected, the 150-nm-thick film was flat and smoothly attached to the support (rms = 5.1 nm) without any buckling (Figure 6a). In water at pH 7, as a bad solvent, the carpet displays strong buckling due to the polymer-brush collapse and the roughness increased significantly to an rms value of 273 nm (Figure 6b). Repetitive solvent exchange (3 times) of neutral water/ethanol showed that the response of the carpet by dramatic change of the layer morphology was completely reversible without any noticeable defects appearing in the supported film. P4VP is also pH sensitive; at a pH below its pK_a of 5.5, the pyridine group of the P4VP brush is protonated and water becomes a good solvent. As shown in Figure 6c, when switching the pH from 7 to 2.5, the layer readily responds by a buckling/unbuckling transition. As the polymer carpets have a thickness of only 150 nm but a macroscopic lateral dimension, the morphology transition is also observable by the naked eye. For better visualization (Figure 6a–c, top photographs), we placed the P4VP carpets on glass slides. Smooth carpets appear transparent and almost invisible and the buckled carpets under bad-solvent conditions become opaque when submerged in a bad solvent (water pH 7) because of light scattering/diffraction at the rough solvent–polymer–surface interfaces. By visual inspection, we determined the switching of the carpet morphology to be instantaneous (subsecond time-scale) upon change of the solvent quality. This fast, visible, and completely reversible reaction of the polymer carpets to a (chemical) stimulus could be applied for the development of new types of actuators, sensors, or displays.

Because of the robustness of the polymer carpets, they can also be prepared, investigated, and used without a solid support. Freestanding polymer carpets with thicknesses of between 10 and 200 nm were prepared by SIPGP of styrene on 5×5 mm² cABT nanosheets supported by silicon wafers with a 100-nm-thick sacrificial silicon nitride layer. After polymerization and removal of ungrafted polymer, the intermediate layer was dissolved by an aqueous hydrofluoric acid (HF) solution. The floating 5×5 mm² carpets could be easily transferred onto a copper grid for electron microscopy measurements (Figure 7) or onto a silicon substrate with a single micrometer-sized opening for bulging tests (Figure 8). It is noteworthy that also the freestanding polymer carpets were found to be extremely robust against the various solvent treatments as well as physical stress (transmission electron microscopy (TEM) measurements, ultrahigh-vacuum mechanical and thermal stresses during the mechanical tests, and long storage of several months).

Figure 7 displays a series of images of decreasing scales showing a photograph of the macroscopic PS carpet after transfer to a TEM grid (Figure 7a), an optical micrograph of the carpet edge partly covering a TEM grid (Figure 7b), and a scanning TEM (STEM) image of a TEM-grid opening partially covered with a polymer carpet (Figure 7c). We recognize occasional dark stripes in the polymer carpet that most probably originate from folded carpets during the transfer

Table 1. Wetting experiments (water) on PS carpets of increasing thicknesses with rms values as determined by AFM and the static (θ_s), advancing (θ_a), receding (θ_r), and contact-angle hysteresis ($\Delta\theta$) values.

	Polymerization time [h]	Layer thickness [nm]	Roughness (rms) [nm]	θ_s [deg]	θ_a [deg]	θ_r [deg]	$\Delta\theta$ [deg]
a)	0.5	19 ± 7	1.6	95	95	82	13
b)	1	46 ± 7	2.5	90	99	80	19
c)	2	67 ± 9	11	95	95	75	20
d)	4	138 ± 15	39	95	95	76	19
e)	8	195 ± 30	62	100	105	0	105
f)	16	–	575	135	146	0	146

process. Quantitative analysis of the electron intensities (gray scales) in Figure 6c for uncovered and covered areas allows the calculation of the carpet thickness from the electron transmittance (T) through the polystyrene carpet by a simple equation, $T = (I - I_B)/(I_0 - I_B)$, where I , I_0 , and I_B are the intensities of electrons penetrating the carpet, the uncovered opening, and the copper bar, respectively. If the membrane thickness (h) is known, the electron-attenuation length (which is inversely proportional to the mass density), can be directly derived from T . In Figure 7d, the T values are plotted as a function of the PS-carpet thickness, as measured by AFM. The electron-attenuation length (at 20 kV) of PS carpets was found to be ≈ 37 nm and independent of the layer thickness. This is in agreement with the attenuation length of 20 kV electrons in bulk polystyrene (40 nm)^[36] and it can be concluded that the mass density of the PS carpets is almost identical to that of bulk PS. As outlined above, thick polymer carpets could not be measured accurately by AFM because of the strong buckling. However, direct

determination of the layer thickness is possible by electron-transmittance measurements (Figure 7d).

Figure 7e shows a STEM micrograph of a thick freestanding PS carpet ($d > 100$ nm) that shows strong buckling of the layer. It is noteworthy that stronger buckling was always observed for the freestanding polymer carpets because of the lack of stabilizing surface–film interactions.

The micromechanical behavior of polymer carpets was investigated using a bulging test. PS carpets with different thicknesses were transferred onto a silicon substrate with a rectangular window of $30 \times 40 \mu\text{m}^2$. The samples were mounted onto a home-built pressure cell in an airtight manner,^[8] as shown in Figure 8a. A differential pressure between the two sides of the polymer carpet was applied and the resulting deflection was measured by AFM. Figure 8a shows the pressure–deflection curve of a 15-nm-thick PS carpet. The polymer-carpet pressure response was found to be nonlinear and consistent with theoretical predictions for the elastic deformation of a thin membrane under tension when internal stresses control the mechanical behavior.^[37] The experimental data were fitted to yield the Young's modulus (E) and the membrane's residual stress at zero pressure.^[8] The values of the elastic modulus for PS carpets with various thicknesses using this model were found to be between 2.0 and 3.6 GPa (Figure 8b). These moduli are significantly higher than the values recently reported for highly crosslinked organic/inorganic interpenetrating nanomembranes.^[14] These remarkably large values indicate the absence of significant mechanical defects or chinks (cracks, clefts, or fissures) within the entire freestanding polymer-carpet layer, despite their nanoscale thicknesses down to 10 nm.

Figure 8b shows a clear relation between the Young's modulus and the thickness of the polymer-carpet layer. It must be pointed out that a polymer carpet is a composite membrane consisting of a crosslinked biphenyl monolayer with a soft polymer-brush layer and that the measured elastic modulus is a thickness-weighted average between the two compounds.^[38] Since the Young's modulus of a single 1-nm-thick cABT nanosheet was measured to be 8 GPa, the Young's modulus of the PS component can be calculated (red circles in Figure 8b). For the thinnest polymer carpet, a modulus of 1.3 GPa was found, which is below the bulk PS value of 3.0 GPa.^[39] However, thicker PS carpets reach the Young's modulus of bulk PS. Our findings are in agreement with a recent report on PS brushes on solid substrates by Tsukruk et al.^[40] In addition, they found that the Young's modulus of a PS-brush layer was significantly lower than that of the bulk polymer and also higher values with increasing brush-layer thickness and, finally,

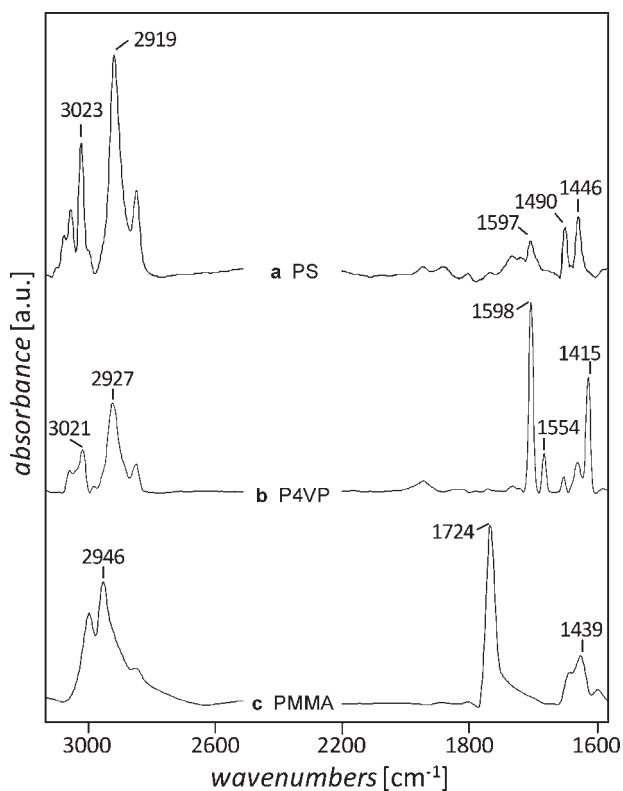


Figure 5. FTIR spectra of different polymer carpets prepared by SIPGP on silicon-supported cABT nanosheets: a) PS (irradiation time, $t_p = 8$ h), b) P4VP ($t_p = 19$ h), and c) PMMA ($t_p = 3$ h).

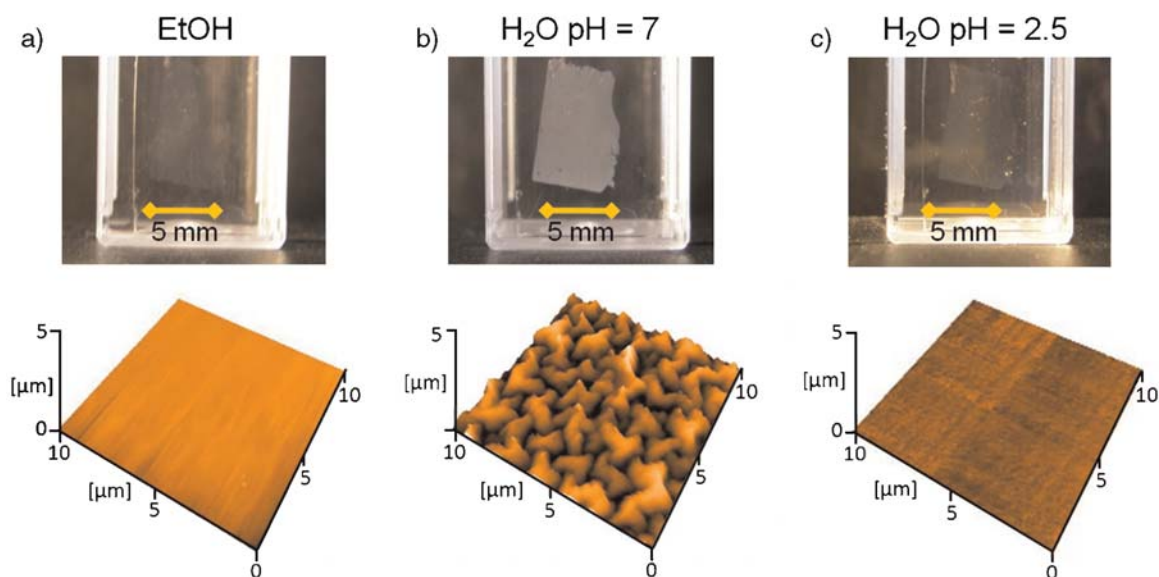


Figure 6. Photographs (above) and AFM measurements (below) of P4VP carpets in a) ethanol, b) water at pH 7, and c) water at pH 2.5.

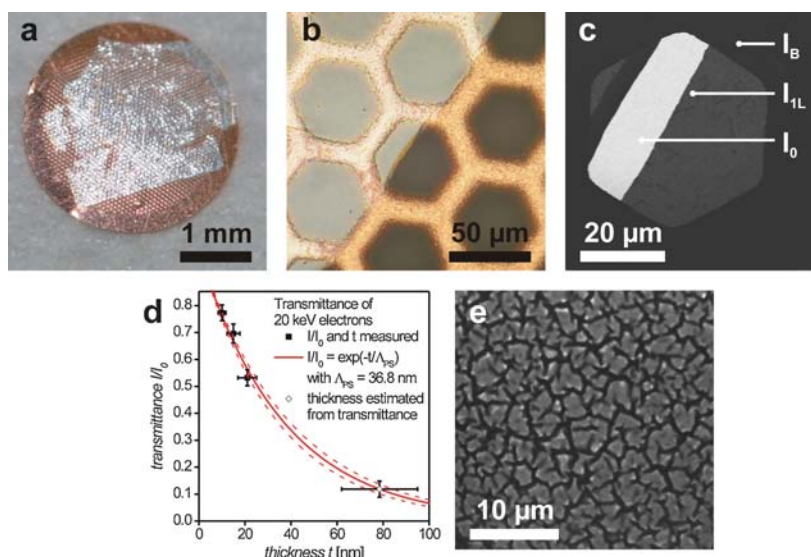


Figure 7. a) Photograph, b) optical micrograph, and c) STEM image of freestanding PS carpets. d) The transmittance of 20 keV electrons was determined from STEM images of PS-carpet edges, such as in (c). An attenuation length of 36.8 nm (solid red line) \pm 2.6 nm (dashed lines) was calculated. e) STEM image of a freestanding PS carpet at higher magnification.

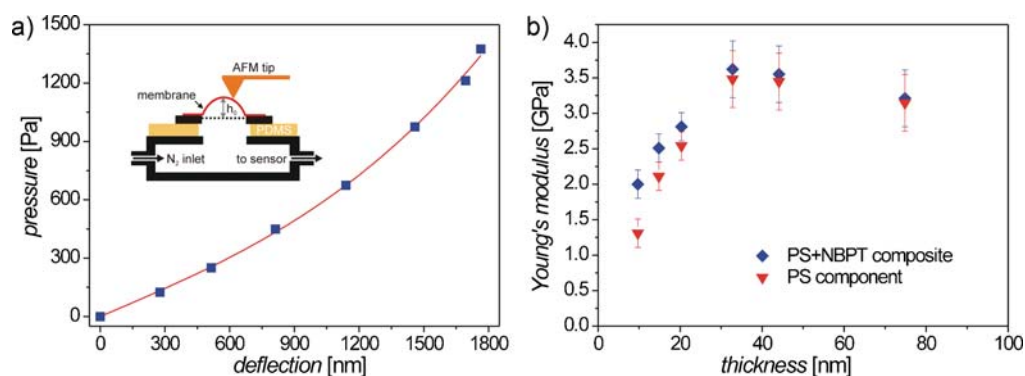


Figure 8. Bulge tests with freestanding polymer carpets yield their Young's modulus. a) The applied pressure as function of the carpet deflection (squares) follows the calculated dependency of thin membranes under tension^[38] (line) and allows the extraction of the Young's modulus.

saturation at the bulk value of PS were measured. It is believed that the ordering of the polymer chains in a brush morphology with lower polymer-chain entanglement and the spatial constraints within the layer are responsible for the specific mechanical properties for thin brush layers. These experiments corroborate the brush morphology of the polymer carpets and demonstrate that the micromechanical properties of free-standing polymer carpets can be systematically controlled by, for example, varying the polymer-brush-layer thickness by the SIPGP-reaction time.

3. Conclusions

In summary, we have shown for the first time the preparation of supported and freestanding polymer carpets, which are brushes directly grafted from crosslinked nanosheets. Polymer carpets exhibit remarkable and unprecedented properties combining extreme thinness, mechanical and chemical stability, robustness, flexibility, and (chemical) sensitivity. Moreover, it was found that the morphology of polymer carpets quickly and reversibly responds to solvent quality and pH by buckling and significant change of their physical properties (i.e., optical characteristics and wetting). This cooperative change of the entire layer morphology may be applied for the development of integrated nano-/micromechanical systems, such as actuators or sensors. Because of the high aspect ratio spanning several dimensions (nanometer thickness and micro-to-centimeter sheets), devices that couple minute changes to macroscopic effects are possible. Furthermore, the simple two-step procedure (electron-induced SAM cross-linking followed by SIPGP) for the preparation of polymer carpets allows the introduction of multiple chemical functionalities within the layer by varying the monomer and/or by polymer analogue reactions.^[25,26] We showed that the polymer-carpet thickness, as well as its mechanical properties, can be precisely and easily tuned by varying the polymerization time. While, in this work, we focused on the synthesis and characterization of macroscopic and homogeneous polymer carpets, the two-step approach can potentially be applied for the fabrication of structured, mixed, as well as gradient polymer carpets on the micrometer and nanometer scale, analogously to our recent accounts on SIPGP on crosslinked SAMs. This will further expand the variability and scope of this new class of materials.

4. Experimental Section

Nanosheets: The preparation of crosslinked SAMs employed the recently described procedures.^[41] First, mica substrates with a layer of 300-nm thermally evaporated Au were cleaned in a UV/ozone cleaner (UVOH 150 LAB, FHR, Germany) for 3 min, rinsed with ethanol, and blown dry in a stream of nitrogen. They were then immersed in a 10 mM solution of 4'-nitro-1,1'-biphenyl-4-thiol (NBPT; purchased from Taros Chemicals) or 1,1'-biphenyl-4-thiol (BPT; purchased from Platte Valley Scientific) in *N,N*-dimethylformamide (DMF p.a., purchased from VWR) dried with a 0.4-nm molecular sieve at room temperature for 3 days.

Subsequently, the samples were rinsed with DMF and ethanol (p.a., purchased from VWR) and finally dried in a stream of nitrogen. Crosslinking was achieved in high vacuum ($<5 \times 10^{-7}$ mbar) with an electron floodgun (Specs FG20) at an electron energy of 100 eV and typical dose of 50 mC cm^{-2} for homogeneous SAMs. The dose was measured with a Faraday cup in close proximity to the sample.

The crosslinked SAMs were transferred from the mica substrates to silicon substrates with either a 300-nm-thick oxide layer or a 150-nm-thick silicon nitride layer on top of a 10-nm oxide layer. This transfer was achieved by cleaving the crosslinked SAM from its substrate using a layer of PMMA for stabilization. A ≈ 400 -nm-thick layer of PMMA was spincoated onto the sample and baked on a hotplate. The Au was cleaved from the mica by immersion in hydrofluoric acid (48%) for 5 min and etched away in an I_2/KI etch bath (≈ 15 min). Afterwards, the nanosheet/PMMA was transferred to the silicon substrate, followed by dissolution of the PMMA in acetone, rinsing of the sample with methanol, and drying in a stream of nitrogen.

SIPGP: The silicon-supported nanosheets were submerged into ≈ 1 mL of freshly distilled and degassed styrene, MMA, or 4VP (Fluka) in a glass photoreaction vial. Polymerization was performed under argon atmosphere for different time periods under irradiation with UV light ($\lambda_{\text{max}} = 350$ nm) at room temperature. After the polymerization, the samples were removed from the reaction solution and immediately washed with a good solvent for the respective polymer (PS in toluene; PMMA in acetone; P4VP in ethanol). The samples were additionally cleaned in ethyl acetate and ethanol.

Freestanding nanosheet and carpet fabrication: Freestanding nanosheets and carpets were fabricated by transfer from the substrates with silicon nitride layers onto TEM Cu grids (400 mesh). For that purpose, the polymer/SAM film was cleaved from the substrate by dissolving the silicon nitride layer in hydrofluoric acid (48%).

AFM: AFM scans under ambient conditions were performed with a Nanoscope IIIa scanning probe microscope (Veeco Instruments, Mannheim, Germany) using standard tips in tapping mode under ambient conditions. For the AFM measurements in liquids (water, ethanol) at room temperature, we used a MFP-3D (Atomic Force, Mannheim, Germany) with a standard liquid cell. Scans were performed in tapping mode and with standard tips. Measurements of the Young's modulus of the nanosheets and polymer carpets were performed with a home-made setup, as described previously,^[8] on a NTEGRA AFM system from NT-MDT (Eindhoven, The Netherlands).

Acknowledgements

This work was supported by the Deutsche Forschungsgemeinschaft (DFG) through project JO287/2-1 and the Volkswagenstiftung. Further support by the International Graduate School for Science and Engineering (IGSSE) and the Graduate School for Complex Interfaces (Complnt) at the TU München. M.S. acknowledges support from the Technische Universität

München – Institute for Advanced Study, funded by the German Initiative of Excellence. The authors are thankful to J.-U. Sommer (IPF Dresden, Germany) for fruitful discussions.

- [1] M. B. Shiflett, H. C. Foley, *Science* **1999**, *285*, 1902–1905.
- [2] A. Rogalski, *Progr. Quant. Electron* **2003**, *27*, 59–210.
- [3] X. Wang, C. Drew, S. H. Lee, K. J. Senecal, J. Kumar, L. A. Samuelson, *Nano Lett.* **2002**, *2*, 1273–1275.
- [4] W. T. Huck, A. D. Stroock, G. M. Whitesides, *Angew. Chem. Int. Ed.* **2000**, *39*, 1958–1960.
- [5] F. Mallwitz, A. Laschewsky, *Adv. Mater.* **2005**, *17*, 1296–1299.
- [6] F. Mallwitz, W. A. Goedel, *Angew. Chem. Int. Ed.* **2001**, *40*, 4645–4648.
- [7] W. Eck, A. Küller, M. Grunze, B. Völkel, A. Götzhäuser, *Adv. Mater.* **2005**, *17*, 2583–2587.
- [8] A. Turchanin, A. Beyer, C. T. Nottbohm, X. Zhang, R. Stosch, A. Sologubenko, J. Mayer, P. Hinze, T. Weimann, A. Götzhäuser, *Adv. Mater.* **2009**, *21*, 1233–1237.
- [9] C. Nardin, M. Winterhalter, W. Meier, *Langmuir* **2000**, *16*, 7708–7712.
- [10] J. Mattsson, J. A. Forrest, L. Borjesson, *Phys. Rev. E* **2000**, *62*, 5187–5200.
- [11] C. Jiang, S. Markutsya, Y. Pikus, V. V. Tsukruk, *Nat. Mater.* **2004**, *3*, 721–728.
- [12] H. Ko, C. Jiang, H. Shulha, V. V. Tsukruk, *Chem. Mater.* **2005**, *17*, 2490–2493.
- [13] H. Watanabe, R. Vendamme, T. Kunitake, *Bull. Chem. Soc. Jpn.* **2007**, *80*, 433–440.
- [14] R. Vendamme, S. Y. Onoue, A. Nakao, T. Kunitake, *Nat. Mater.* **2006**, *5*, 494–501.
- [15] E. T. Carlen, M. S. Weinberg, C. E. Dubé, A. M. Zapata, J. T. Borenstein, *Appl. Phys. Lett.* **2006**, *89*, 173123.
- [16] C. Stampfer, T. Helbling, D. Obergfell, B. Schoberle, M. K. Tripp, A. Jungen, S. Roth, V. M. Bright, C. Hierold, *Nano Lett.* **2006**, *6*, 233–237.
- [17] Z. Tang, N. A. Kotov, S. Magonov, B. Ozturk, *Nat. Mater.* **2003**, *2*, 413–418.
- [18] O. Yosuke, K. Koki, K. Manabu, S. Daizoh, T. Shinji, *Adv. Mater.* **2009**, *21*, 4388–4392.
- [19] R. Ducker, A. Garcia, J. Zhang, T. Chen, S. Zauscher, *Soft Matter* **2008**, *4*, 1774–1786.
- [20] *Surface-Initiated Polymerization I & II* (Ed: R. Jordan), Advances in Polymer Science, Vol. 197 & 198, Springer, Heidelberg **2006**.
- [21] *Polymer Brushes* (Eds: R.C. Advincula, W. J. Brittain, K. C. Caster, J. Rühe) Wiley-VCH, Weinheim **2004**.
- [22] E. M. Sevick, D. R. M. Williams, *Macromolecules* **1994**, *27*, 5285–5290.
- [23] A. Kumar, A. Srivastava, I. Y. Galaev, B. Mattiasson, *Prog. Polym. Sci.* **2007**, *32*, 1205–1237.
- [24] M. Steenackers, A. Küller, S. Stoycheva, M. Grunze, R. Jordan, *Langmuir* **2009**, *25*, 2225–2231.
- [25] M. Steenackers, R. Jordan, A. Küller, M. Grunze, *Adv. Mater.* **2009**, *21*, 2921–2925.
- [26] M. Steenackers, S. Q. Lud, M. Niedermeier, P. Bruno, D. M. Gruen, P. Feulner, M. Stutzmann, J. A. Garrido, R. Jordan, *J. Am. Chem. Soc.* **2007**, *129*, 15655–15661.
- [27] a) N. Zhang, M. Steenackers, R. Luxenhofer, R. Jordan, *Macromolecules* **2009**, *42*, 5345–5351; b) N. A. Hutter, A. Reitingner, N. Zhang, M. Steenackers, O. A. Williams, J. A. Garrido, R. Jordan, *Phys. Chem. Chem. Phys.* **2010**, *12*, 4360–4366.
- [28] J. Genzer, J. Groenewold, *Soft Matter* **2006**, *2*, 310–323.
- [29] J. Groenewold, *Physica A* **2001**, *298*, 32–45.
- [30] Z. Y. Huang, W. Hong, Z. Suo, *J. Mech. Phys. Solids* **2005**, *53*, 2101–2118.
- [31] E. A. Wilder, S. Guo, S. Lin-Gibson, M. J. Fasolka, C. M. Stafford, *Macromolecules* **2006**, *39*, 4138–4143.
- [32] D. R. M. Williams, *J. Phys. II* **1993**, *3*, 1313–1318.
- [33] C. Yeung, A. C. Balazs, D. Jasnow, *Macromolecules* **1993**, *26*, 1914–1921.
- [34] H. Wang, H. R. Brown, *Macromol. Rapid Commun.* **2004**, *25*, 1095–1099.
- [35] J. Deng, W. Yang, B. Ranby, *Macromol. Rapid Commun.* **2001**, *22*, 535–539.
- [36] S. M. Pimblott, J. A. LaVerne, A. AlbaGarcia, L. D. A. Siebbeles, *J. Phys. Chem. B* **2000**, *104*, 9607–9614.
- [37] J. J. Vlassak, W. D. Nix, *J. Mater. Res.* **1992**, *7*, 3242–3249.
- [38] P. Martins, P. Delobelle, C. Malhaire, S. Brida, D. Barbier, *Eur. Phys. J. Appl. Phys.* **2009**, *45*, 10501.
- [39] *Polymer Handbook*, 3rd ed. (Eds: J. Bandrup, E. H. Immergut), Wiley Interscience, New York **1989**.
- [40] D. Julthongpiput, M. LeMieux, V. V. Tsukruk, *Polymer* **2003**, *44*, 4557–4562.
- [41] A. Beyer, A. Godt, I. Amin, C. T. Nottbohm, C. Schmidt, J. Zhao, A. Götzhäuser, *Phys. Chem. Chem. Phys.* **2008**, *10*, 7233–7238.

Received: March 17, 2010
 Revised: May 10, 2010
 Published online: